

Unveiling the role of catalytically active MXene supports in enhancing the performance and durability of cobalt oxygen evolution reaction catalysts for anion exchange membrane water electrolyzers

Young Sang Park ^{a,b,c,1}, Ari Chae ^{a,d,e,1}, Gwan Hyun Choi ^{a,1}, Swetarekha Ram ^f, Seung-Cheol Lee ^f, Satadeep Bhattacharjee ^f, Jiyoong Jung ^{a,b,c}, Hyo Sang Jeon ^g, Cheol-Hee Ahn ^c, Seung Sang Hwang ^{a,b}, Dong-Yeun Koh ^d, Insik In ^e, Taegon Oh ^{a,b}, Seon Joon Kim ^{a,b}, Chong Min Koo ^{h,i,*}, Albert S. Lee ^{a,b,***}

^a Materials Architecturing Research Center, Korea Institute of Science and Technology, Seoul 02792, the Republic of Korea

^b Convergence Research Center for Solutions to Electromagnetic Interference in Future-Mobility, Korea Institute of Science and Technology, Seoul 02792, Republic of Korea

^c Research Institute of Advanced Materials, Department of Materials Science and Engineering, Seoul National University, Seoul 08826, the Republic of Korea

^d Department of Chemical and Biomolecular Engineering, Korea Advanced Institute of Science and Technology, Daejeon 34141, the Republic of Korea

^e Department of IT-Energy Convergence (BK21 Four), Chemical Industry Institute, Korea National University of Transportation, Chungju 27469, the Republic of Korea

^f Indo-Korea Science and Technology, Center, Korea Institute of Science and Technology, Bangalore 560065, India

^g Technological Convergence Center, Korea Institute of Science and Technology (KIST), Seoul 02792, the Republic of Korea

^h School of Advanced Materials Science and Engineering, Sungkyunkwan University, Seobu-ro 2066, Jangan-gu, Suwon-si, Gyeonggi-do 16419, the Republic of Korea

ⁱ School of Chemical Engineering, Sungkyunkwan University, Seobu-ro 2066, Jangan-gu, Suwon-si, Gyeonggi-do 16419, the Republic of Korea

ARTICLE INFO

Keywords:

MXene

Oxygen evolution catalyst

Anion exchange membrane water electrolyzer

ABSTRACT

The role of 2D transition metal carbides, also known as MXenes, as active catalyst supports in Co-based oxygen evolution reaction (OER) catalysts was elucidated through a combination of experimental and computation electrochemistry. Through facile seeding of commercial Co nanoparticles on three different MXene supports ($Ti_3C_2T_x$, $Mo_2Ti_2C_3T_x$, Mo_2CT_x), Co@MXene catalysts were prepared and their electrochemical properties examined for alkaline OER electrocatalysts. The OER activity enhancement of Co was significantly improved for Mo_2CT_x and $Mo_2Ti_2C_3T_x$ supports, but marginal on the $Ti_3C_2T_x$ in rotating disk electrode and membrane electrode assembly tests. The Co@ Mo_2CT_x exhibited the highest anion exchange water electrolysis performance of 2.11 A cm^{-2} at 1.8 V with over 700 h of stable performance, exceeding previous benchmarks for non-platinum group (non-PGM) metal OER catalysts. The superior performance was attributed to the strong chemical interaction of Co nanoparticle with the Mo_2CT_x MXene support. Insights into the electrochemical and chemical oxidation according to MXene type as related to cell durability, as well as the effect of electrical conductivity and inherent boosting of electrocatalytic activity of Mo-based MXenes elucidated through density functional theory (DFT) calculations helped explain the performance and durability enhancement of Mo-based MXene supports over $Ti_3C_2T_x$ supports.

1. Introduction

Anion exchange membrane water electrolyzers (AEMWEs) possess the tandem advantages of proton exchange membrane water

electrolyzers (PEMWES) and alkaline water electrolyzers (AWE) [1,2], potentially being able to achieve high current density performance due to the use of a non-porous, solid-state membrane without the use of PGM catalysts [3,4]. The reduced corrosivity of the alkaline environment

* Corresponding author at: School of Advanced Materials Science and Engineering, Sungkyunkwan University, Seobu-ro 2066, Jangan-gu, Suwon-si, Gyeonggi-do 16419, the Republic of Korea.

** Corresponding author at: Materials Architecturing Research Center, Korea Institute of Science and Technology, Seoul 02792, the Republic of Korea.

E-mail addresses: chongminkoo@skku.edu (C.M. Koo), aslee@kist.re.kr (A.S. Lee).

¹ These authors contributed equally to this work.



compared to acidic conditions allows the use of transition metal-based catalysts, enabling a wider range of materials to be investigated as both catalyst and catalyst supports [5].

Common support materials for catalysts include carbonaceous materials for electrochemical applications [6] and various metal oxides for heterogeneous thermal catalysts [7], serving common roles of preventing catalyst agglomeration through mechanical stabilization, increasing and maintaining high surface area for prolonged use [8]. In the case of electrocatalysts, carbonaceous supports provide electrical conductivity, a prerequisite to promote charge-transfer at the triple phase boundary [9]. Moreover, catalyst-support interactions may also affect the electrochemical stability of the catalyst, with oxide-based interlayers shown to enhance interaction strength. However, when considering the stability of support materials, high voltage-induced electrochemical corrosion [10] or water-induced chemical oxidation [11] have been pointed out as major challenges for both the oxygen reduction reaction (ORR) catalysts in fuel cells and far more exceeding so for the OER catalysts in electrolyzers.

MXenes are an emergent class of 2D transition metal carbides with wide-ranging properties including high electrical conductivity, mechanical stiffness, high surface area, excellent electrochemical properties, and even biocompatibility [12–14]. MXenes are synthesized through chemical etching of MAX phase ceramics with a structure of $M_{n+1}AX_n$ (M represents an early transition metal, while A is assigned to an element in either the IIIA or IVA group, and X can be either carbon or nitrogen.), leaving a 2D structure of $M_{n+1}AX_n$ with the A group removed [15]. The chemical etching method used during synthesis generates abundant and varied compositions of terminal groups (T_x) on the surface, consisting of hydroxyl ($-OH$), oxygen ($-O$), and/or fluorine ($-F$), resulting in a stable single-layered 2D structure [16]. Their exceptional electrochemical charge-transfer properties have rendered them advanced materials for supercapacitors, various types of batteries, and as electrocatalysts [17,18].

MXenes have been studied as electrocatalyst support materials, due to their unique properties, such as excellent electrical conductivity, large surface area, abundance of surface termination groups and consequently exceptional electrochemical charge-transfer properties [14]. Recent studies have demonstrated that transition metal oxide-decorated MXenes with different transition metal compositions, such as Mo_2C , $Mo_2Ti_2C_3$, Mo_2TiC_2 and Ti_3C_2 , can enhance the OER activity and durability compared to bare oxides [19]. This has been attributed to the interfacial electronic coupling effect between the decorated transition metal oxide and MXene layers, which promotes electron transfer processes and facilitates the formation of active sites for the OER [20]. And yet to date, there have been no comprehensive studies that have conducted to understand the OER performances of various MXenes with distinct atomic compositions, surface terminations, and electrical conductivities in an “apples to apples” manner.

In this study, we sought out to investigate the role of MXenes as OER electrocatalyst support by seeding a commercial cobalt nanoparticle cluster onto three different MXenes ($Ti_3C_2T_x$, $Mo_2Ti_2C_3T_x$, Mo_2CT_x) and examining their electrochemical properties in both half-cell and membrane electrode assemblies (MEAs) to formulate an overarching rationale for designing MXenes as catalytically active supports.

2. Experimental

2.1. Materials

Ti_3AlC_2 (particle size < 38 μm), Mo_2Ga_2C (particle size < 38 μm) and $Mo_2Ti_2AlC_3$ (particle size < 38 μm) powders were purchased from Jilin 11 Technology Co., Ltd. (ChangChun, China). Lithium fluoride (LiF, 98.5%), cobalt nanopowder (Co (core, 90–95%) Co_3O_4 (shell, ≥ 10 –20%), 99.8%), PtRu/C (Pt 50 wt%, Ru 25 wt%, C 25 wt%) were purchased from Alfa Aesar (Ward Hill, MA, USA). Hydrochloric acid (HCl, 37%), potassium hydroxide (KOH, 95%), n-propyl alcohol (NPA)

and all other solvents were purchased from Daejung Chemicals & Materials Co., Ltd. (Siheung-si, Republic of Korea). Hydrofluoric acid (HF, 48%) and tetramethylammonium hydroxide solution (TMAOH, 25 wt% in H_2O) were purchased from Sigma-Aldrich (St. Louis, MO, USA). Carbon paper (36 BB), poly-norbornene anion exchange membrane, Xion Penton-72–15CL from Fuel Cell Store Co., Ltd (Texas, USA), platinized titanium porous transport layer (PtTi PTL, Giner, USA) were used as received. Deionized water was produced using a laboratory system (Aqua puri series, Youngin Chromass).

2.2. Preparation of MXene supported Co OER catalysts

2.2.1. Synthesis of MXenes

MXenes were synthesized using the well-known HF etching method of MAX powders, where each reaction time and amount of etchant were varied. [21,22] Specifically, 1 g of Ti_3AlC_2 was etched in a 20 mL solution of 5 wt% HF at room temperature for 24 h, while 1 g of Mo_2Ga_2C was etched in a 20 mL solution of 25 wt% HF at room temperature for 160 h. Additionally, 1 g of $Mo_2Ti_2AlC_3$ was etched in a 20 mL solution of 48 wt% HF at room temperature for 96 h. The resulting products were washed with distilled water until neutralized, utilizing centrifugation.

To delaminate the multi-layered MXenes into single-layered MXenes, 1 g of each MXene was mixed separately in a 100 mL solution of 10 wt% TMAOH at room temperature for 12 h [22]. The basic mixtures were then washed until neutralized using centrifugation, and the solution was centrifuged at a 3500 rpm to collect the supernatant for the stable single-layered MXene. Finally, the synthesized MXene solutions were freeze-dried to obtain MXene powders.

2.2.2. Synthesis of Co@MXenes

In this study, commercial Co nanoparticles (Co NP) as well as their hybrids with MXene supports (hereafter referred to as Co@MXene) including Mo_2CT_x , $Mo_2Ti_2C_3T_x$, and $Ti_3C_2T_x$ were synthesized using a simple physical mixing method, and their OER performance was evaluated using electrochemical techniques to investigate the role of MXene supports in enhancing OER performance. First, 80 mg of Co NP and 80 mg of MXene were mixed in equal weight ratio (50 wt% Co) in 100 mg of distilled water and 20 g of n-propyl alcohol. To make a well-dispersed solution, the sample was sonicated in ultra-sonication bath (KODO, JAC 3010) for 1 h maintaining the temperature less than 20 °C to minimize the oxidation of MXene. Then, the above solution was transferred into a crucible container and temperature was kept at 200 °C for 1 h under Ar atmosphere. The obtained powder was stored in a dessicator (0.1 kPa) for further experiments. All Co@MXene catalysts were fabricated in the same method.

2.3. Synthesis of trimethyl ammonium functionalized polystyrene ionomer (TMA-70)

To synthesize trimethyl ammonium functionalized polystyrene ionomers (TMA-70), polyvinylbenzyl chloride (2 g) was dissolved in DMSO (60 mL), and 45% Trimethylamine aqueous solution (1.33 mL) was added. After stirring for 3 h at room temperature, add 2-(4-fluorophenyl)ethylamine (0.586 g) and stirring at 80 °C for 12 h. Polymer was precipitated in a mixture of tetrahydrofuran (THF) and ethyl acetate (EA) 1:1 (v/v), dissolve in methanol again, and re-precipitate in EA. The obtained powder is treated with 1.0 M NaOH, washed with distilled water, and vacuum dried. The obtained TMA-70 was dissolved in H_2O and IPA 1:1 (v/v) at 5 wt% to prepare an ionomeric binder solution [2].

2.4. Materials characterizations

To analyze the molecular structure of ionomer, 600 MHz 1H nuclear magnetic resonance equipment (NMR, DD2 600 MHz, Agilent Technologies) was used. Powder X-ray diffraction (XRD) patterns were obtained (D/MAX-2500-PC, Rigaku) using Cu $K\alpha$ radiation in the 2 theta

range from 3° to 70° with a step size of 2.0° min⁻¹. Surface morphologies, interface structures, and chemical compositions were observed by using high resolution transmission electron microscopy (HR-TEM, Tecnai F20 G2, FEI), scanning electron spectroscopy (SEM, FEI, Teneo VS), and corresponding energy dispersive X-ray spectroscopy (EDS) for elemental analysis. X-ray photoelectron spectroscopy (XPS, PHI 5000 VersaProbe, Ulvac-PHI) was used to determine chemical compositions. X-ray adsorption fine structure (XAES, synchrotron radiation based measurement) experiment was conducted in transmittance and fluorescence (for in-situ experiment) mode under ambient conditions on the 1D (XRS KIST-PAL) beamline of Pohang Light Source-II (PLS-II). The monochromatic beam was detuned (to 80% of maximum intensity for Co K-edge) to eliminate higher order harmonics using Si (111) double-crystal monochromator. The spectra were calibrated with the first inflection points (i.e., Co K-edge = 7723 eV) in the spectra of reference metal foils and normalized using Artemis program. The normalized EXAFS signal was weighted by k^3 to magnify high-energy oscillations and the Fourier-transformed in a k -range of 2.0–10.0 Å.

2.5. Electrochemical testing

2.5.1. Rotating disk electrode (RDE) experiments

The ink used in this study was prepared by mixing a certain composition of ionomer, catalyst, and solvent. First, the ionomer TMA-70 was dissolved in ethanol to form a 5 wt% solution. Next, the Co NP or Co@MXene catalyst material was added to the solution at a 10 wt% weight ratio and sonicated for 30 min to ensure a uniform dispersion. The ink was then deposited onto a glassy carbon electrode (GCE) with an appropriate loading level. The GCE was first polished with 0.05 µm alumina slurry and rinsed with deionized water and ethanol. A small amount of the ink was then drop-cast onto the surface of the GCE, and the electrode was dried under ambient conditions. The loading level of the catalyst material was controlled by adjusting the amount of ink deposited onto the GCE surface. Next, the prepared GCE with the deposited catalyst material was immersed in an electrolyte solution (e.g. 1.0 M KOH) and used as the working electrode. A graphite rod and a Hg/HgO electrode were used as the counter and reference electrodes, respectively. The OER performance of the catalyst was then measured by sweeping the potential from an initial potential (e.g. 0.9 V vs. RHE) to a final potential (e.g. 1.7 V vs. RHE) at a scan rate of 10 mV s⁻¹ and rotating speed of 1600 rpm. The resulting current densities were recorded and used to calculate the electrocatalytic activity of the catalyst material.

2.5.2. MEA testing

MEAs with 1 cm² active area were fabricated by catalyst coated substrate (CCS) method. Co NP or Co@MXenes was used as anode and PtRu/C were used as cathode catalysts, respectively. Catalyst inks were prepared by dispersing each catalyst powder over the TMA-70 ionomer, which was synthesized using a literature procedure [2] (Fig. S1) (4.65 wt% TMA-70 solution in n-propanol: water 5:5 weight ratio co-solution, the ionomer to carbon (I/C) weight ratio is 0.2, and for the OER, and HER catalyst layer the binder content was 10 wt%) in an aqueous solution of n-propanol and small amount of water, followed by ultrasonic treatment for more than 20 min with maintaining water temperature less than 30 °C to prevent catalyst agglomeration. The prepared catalyst inks were directly sprayed onto the PTL set on a 70 °C preheated hot plate. Carbon paper were used for cathode and PtTi as the anode PTL. Cathode catalyst loading was 0.6 mg_{Pt} cm⁻², while the anode catalyst loading amount normalized at 0.7 mg_{Co} cm⁻². The fabricated CCS was dried at room temperature for more than 1 h to remove residual solvent in the catalyst layer. Xion Pention-72–15CL (thickness 30 µm) was used as an anion exchange membrane. Prior to single cell application, the membranes were sandwiched by the fabricated electrode without hot-pressing process. Polarization curves were obtained with Scribner electrolyzer cells with power supplied by Biologic potentiostat (SP-200)

attached to 30 A power booster (HCV-3048) with 80 °C, 1.0 M KOH electrolyte supplied by a peristaltic pump.

2.6. Calculations of the H₂ Faradaic efficiency (FE), H₂ production rate, and energy conversion efficiency (ECE)

The hydrogen gas product was quantified by gas chromatography (GC, Agilent 6890 N) equipped with a thermal conductivity detector (TCD) using He (99.9999%) as the carrier gas. The GC was directly connected to the MEA for on-line analysis using a six-port valve system. The FE for hydrogen product was determined by computing the areas of the GC chromatogram as indicated below [8]:

$$i_{\text{partial}} = V \times \text{flow rate} \times \frac{nFp_0}{RT}$$

$$\text{FE (\%)} = \frac{i_{\text{partial}}}{i_{\text{total}}} \times 100$$

The parameter V denotes the gas product's volume concentration as determined by the previous calibration of the gas chromatograph (GC), while the flow rate (mL min⁻¹) was determined using a universal flow meter (ADM 1000, Agilent Technologies). n is the number of transferred electrons for a H₂ product, i_{total} (mA) is a steady-state current, T represents the temperature, $F = 96,485$ (A·s mol⁻¹), $p_0 = 1.013$ (bar), and $R = 8.3145$ (J mol⁻¹ K⁻¹).

The hydrogen production rate is calculated as follows.

$$V_{\text{H}_2 \text{ production rate}} (L \text{ h}^{-1} \bullet \text{cm}^{-2}) = j \times \frac{H_2 \text{ FE (\%)}}{100 (\%)} \times \frac{n_{e^-} / 2 \times V_{n, \text{H}_2}}{N_A}$$

where j is current density (A cm⁻²), H_2 FE is Faradaic efficiency of hydrogen, n_{e^-} is the number of electrons reacted at 1 A per hour (2.247 × 10²², A⁻¹·h⁻¹), V_{n, H_2} is the volume of hydrogen per mol (22.4 L mol⁻¹), N_A is the Avogadro's number (6.02 × 10²³ mol⁻¹).

The ECE is calculated as follows [23].

$$\text{ECE (\%)} = \frac{E_{\text{Output}}}{E_{\text{Input}}} = \frac{V_{\text{H}_2} \bullet H_0}{W_h} \times 100$$

where V_{H_2} is the volume of H₂ per hour (m³ h⁻¹), H_0 is the calorific value of hydrogen (10.8 × 10⁶ J m⁻³, lower heating value), W_h is the electric power to produce hydrogen for an hour.

3. Results and discussion

3.1. Design rationale for Co@MXenes catalyst

The design rationale of Co seeded MXenes lies in our interest to understand the role of MXenes as electrocatalyst support. As Co is commonly known to be a good OER catalyst and the commercial Co NP clusters utilized in our study has been reported by many to show practical performance in both half-cell and MEAs, we seeded Co on three different MXenes of Ti₃C₂T_x, Mo₂Ti₂C₃T_x, and Mo₂CT_x. The selection of MXenes was in part to evaluate both the surface metal group Mo vs Ti, as well the wide-ranging electrical conductivities of these materials; Ti₃C₂T_x, Mo₂Ti₂C₃T_x, Mo₂CT_x are known in literature of having electrical conductivities of 2650, 227, 0.8 S cm⁻¹ [24–26]. Moreover, while the vast majority of studies of MXenes have been centered on Ti₃C₂T_x, we selected to investigate the effect of atomic variance of MXenes as such tuning may give rise to a greater understanding of how MXenes are able to potentially increase the inherent catalytic activity of a catalyst, a trait that is rarely accomplished with other types of catalyst supports such as carbon or metal oxides. As such, in our material selection and design of commercial Co active material and atom controllable MXenes, we were able to systematically evaluate the role and effect of metal surface site for catalyst-MXene interactions, electrical conductivity, as well as electrochemical or chemical oxidation in a clear manner. Co

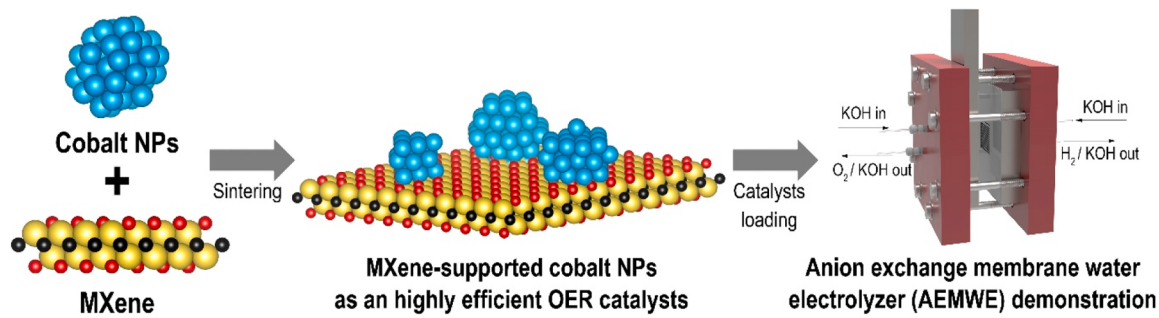


Fig. 1. Schematic description of fabrication and evaluation process of Co@MXene catalyst applying anion exchange membrane water electrolyzer OER.

nanoparticle (Co, core, 90–95%/Co₃O₄, shell, 10–20%), which has a core-shell structure (product's specification sheet), was characterized to Co oxide (XRD, XPS) or Co metallic component (XAS) depending on the depth of the characterized method's light source. We referred the each catalyst samples as a Co NP or Co@MXene(Co@Mo₂CT_x, Co@Mo₂Ti₂C₃T_x, Co@Ti₃C₂T_x) generally to prevent confusion to the readers with the accurate information.

3.2. Characterization of pristine MXenes and Co@MXenes

The structure and phase of MXenes and Co@MXenes were investigated using XRD, as shown in Fig. 2(a) and Fig. S2. The presence of (00_l) peaks in the XRD patterns of MXene nanosheets indicate the successful synthesis of MXenes from the corresponding MAX ceramics through chemical etching and delamination (Fig. S2(a)) [21]. In Fig. S2(b), the same crystalline peaks in the XRD patterns before and after sintering at a

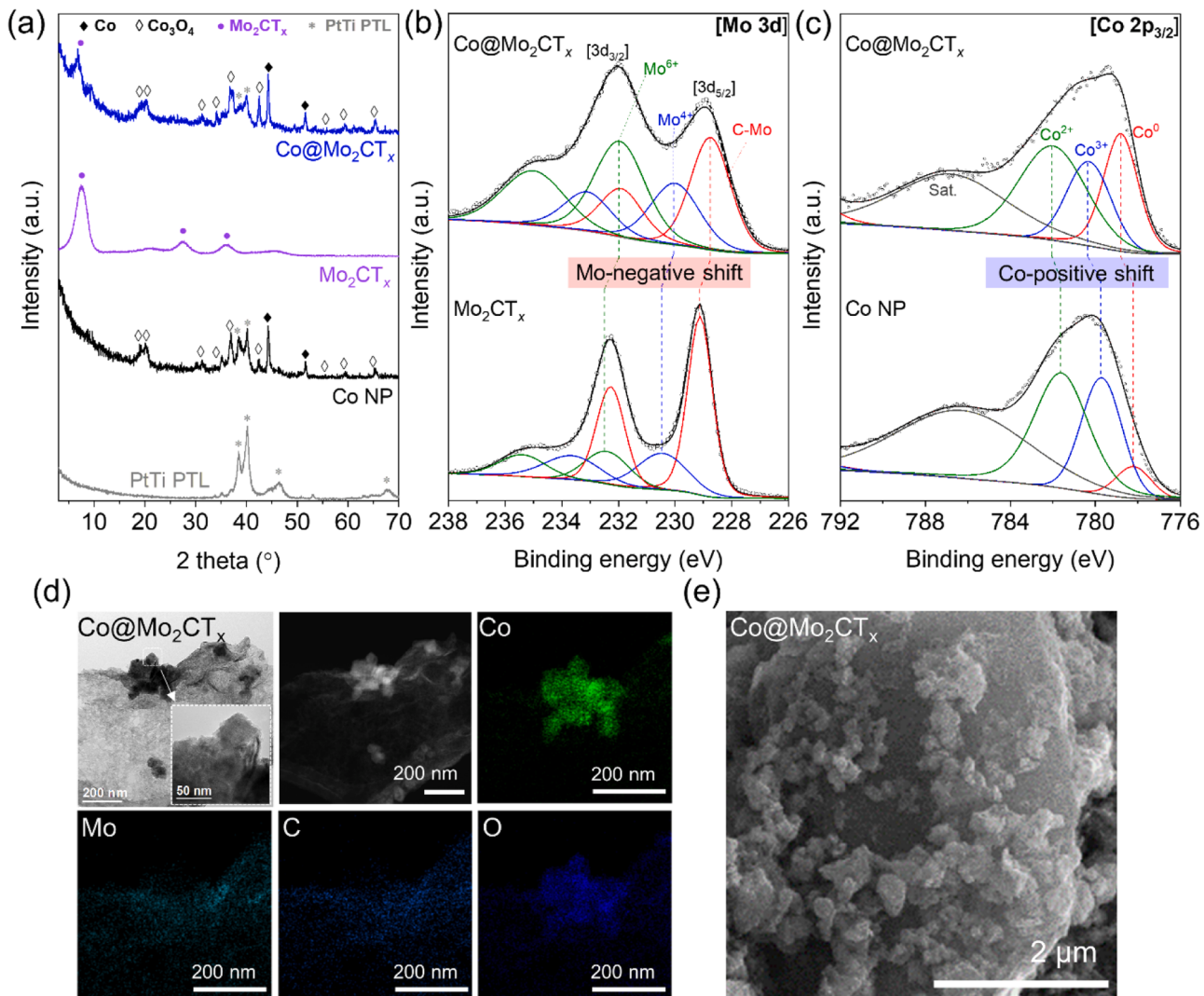


Fig. 2. Characterization of MXene and Co@MXene catalysts. (a) XRD patterns of platinized titanium PTL, pristine MXene without PTL, and Co NP, Co@Mo₂CT_x spray-coated on PtTi PTL, XPS profiles of (b) Mo 3d, and (c) Co 2p, (d) TEM image of Co@Mo₂CT_x catalyst, and EDS mapping. SEM image of fabricated Co@Mo₂CT_x catalyst.

temperature of 200 °C indicate that Co NPs exhibit no structural differences after the sintering process for fabrication of Co@MXene hybrid. The XRD pattern of the fabricated Co@Mo₂CT_x electrode shows both the (00 l) peak of Mo₂CT_x MXene and the co-exist of crystalline Co and Co₃O₄ phase of Co NP, indicating the successful hybridization of the two materials (Fig. 2(a)). In Fig. S2(c), the XRD patterns of Co@MXene hybrid electrode exhibited unique MXene peak, crystalline phases of Co NPs, and PtTi PTL substrates, regardless of the different types of MXene used.

The electronic properties and valence state of the elements were investigated through XPS analysis. All XPS peaks were calibrated using C-C binding energy of C1s (284.6 eV). The Mo3d XPS profile of the Mo₂CT_x MXene showed three pairs of doublets (Mo3d 3d_{5/2}, Mo3d 3d_{3/2}) with an area ratio of 0.7 and separation of 3.1 eV (Fig. 2(b)) [27,28]. The Mo 3d high-resolution spectrum of Mo₂CT_x MXene exhibits peaks at 229.1, 230.5, and 232.5 eV corresponding to Mo-C, Mo⁴⁺, and Mo⁶⁺ states, respectively, while the Co@Mo₂CT_x hybrid exhibits peaks at 228.8, 230.1, and 232.0 eV. The binding energy of Co@Mo₂CT_x hybrids shift to lower binding energies (\approx 0.4 eV) compared to MXene, indicating the formation of strong chemical bonding interaction between Co NP and Mo₂CT_x [29,30]. It is noteworthy to point out that we found evidence of MXene oxidation or defects formed during the sintering processes. While unintended, the presence of defects and oxidation sites were mostly likely sites to which Co NP could effectively seed. The presence of a chemical bond, as will be discussed in later sections, enables the spontaneous charge transfer from Co NP to Mo₂CT_x. The Co 2p high-resolution spectrum of the Co@Mo₂CT_x provides support for this assumption (Fig. 2(c)). In the Co 2p_{3/2} high-resolution spectra of Mo₂CT_x MXene and Co NP, four-deconvoluted peaks corresponding to Co⁰, Co³⁺, Co²⁺, and satellite were observed. The Co⁰ peak of Co NP showed a higher binding energy shift from 778.2 to 778.8 eV in the Co@Mo₂CT_x hybrid. This phenomenon increases the positive charge of the Co center, enhancing the electrostatic attraction to the additional anionic intermediate and consequently promotes faster redox processes in an alkaline medium [31,32]. The shifted binding energy of the Co@Ti₃C₂T_x, Co@Mo₂Ti₂C₃T_x and Co@Mo₂CT_x hybrids in XPS spectra indicates the formation of new chemical bonds (Fig. S3).

The morphologies and structures of Co@MXenes were characterized through SEM and TEM measurements. In Fig. S4, the TEM images and selected area electron diffraction (SAED) patterns reveal a high hexagonal crystalline order, confirming the monocrystalline single-layered structure of the MXene. TEM images and EDS mapping analysis in Fig. 2(d) have confirmed that the particles observed on the surface and edge sites of Co@Mo₂CT_x are indeed Co NPs. In Fig. 2(e), the SEM image of the fabricated AEMWE anode substrate coated with Co@Mo₂CT_x showed an abundant amount of randomly distributed Co NPs. The distribution of Co NPs in Co@Ti₃C₂T_x and Co@Mo₂Ti₂C₃T_x hybrids was confirmed to be non-uniform, similar to that observed in Co@Mo₂CT_x (Fig. S5). The randomly clustered morphology may also be a manifestation of the high Co NP loading (50 wt%) on MXenes.

XAES spectroscopy was employed to accurately demonstrate local structural, and chemical state information of catalytic active site cobalt to elucidate the Co-MXene interaction. First, Co K-edge X-ray absorption near edge structure (XANES) in Fig. 3(a) showed different absorption edge energies among different Co@MXenes compared to Co NP, as the Co@Mo₂CT_x surface shows a higher oxidation state than cobalt on the Ti surface. Even with the identical Mo surface, Mo₂CT_x has a slightly lower oxidation state than Mo₂Ti₂C₃T_x. This trend verifies the differing chemical interactions between Co and MXene through different oxidation state. Moreover, cobalt NPs located on each surface of each MXene have different interaction along interface of each MXene. The local environment of cobalt in each MXene was then probed by Co K-edge Fourier-transformed extended X-ray absorption fine structure (FT-EXAFS) as shown in Fig. 3(b), with the Co@MXenes exhibiting a starkly differing structure compared to cobalt NP, demonstrating the chemical bonding of Co and MXene to form a unique heterostructure as indicated

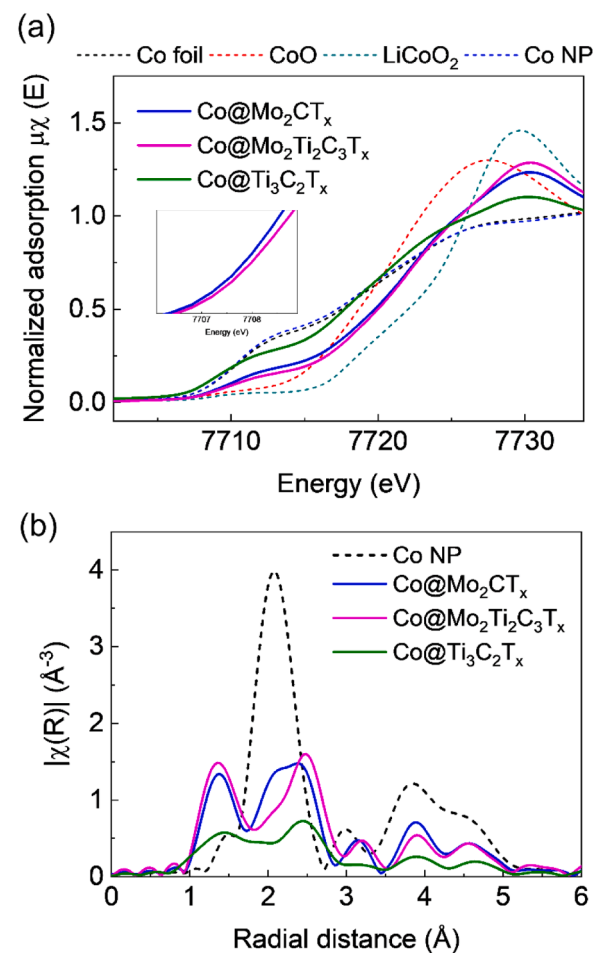


Fig. 3. XAFS normalization profiles of Co K-edge (a) XANES. (b) FT-EXAFS of Co NP, and Co@MXene catalysts.

by the Co-Mo interaction showing red shift of Co-Co (\approx 2–2.1 Å) and Co-Ti interaction (\approx 1.4 Å) [33,34]. As peak broadening can occur due to interference from small differences in atomic environment from the presence of more than one material phase while peak amplitude is generally affected by the number of bonds as well as the distance between the central atom and surrounding atoms, we compared the local environments of Co and sintered Co, which showed no change in crystal structure (Fig. S2(b)) [35]. Thus the change between each sample's FT-EXAFS signal must be the cobalt and surface of MXene interaction. The wavelet transform (WT) of k_3 -weighted EXAFS signals was performed to quantitatively compare the atomic distribution information with respect to the R -space (radial space) and k_3 -space (energy space) and consequently gain a comprehensive understanding of the atoms surrounding the central atom. The WT of EXAFS signals are beneficial for distinguishing the different types of atoms within one atomic shell; the EXAFS signals of different atomic components cannot be effectively separated through the conventional Fourier transform (FT) approach. After WT, distinctly different intensity profiles were obtained of Co NP containing metallic Co and Co₃O₄ and each Co@MXene samples on Fig. S6. These results clearly suggest that Co particles form strong chemical bonding interactions with MXene surface atoms in the Co@Mo₂CT_x, Co@Mo₂Ti₂C₃T_x, and Co@Ti₃C₂T_x hybrids.

3.3. Electrochemical properties

The development of efficient electrocatalysts for OER is critical for the advancement of sustainable energy technologies. Cobalt has been regarded as a promising non-PGM OER catalyst for alkaline water

electrolysis [36]. However, its catalyst performance can be influenced by the types of catalyst-support interactions. As shown in Fig. 4(a), linear sweep voltammetry (LSV) was used to measure the polarization curves of the samples using a RDE test, and the overpotential required to achieve a current density of 10 mA cm^{-2} was measured. Notably, Co@Mo₂CT_x exhibited the lowest overpotential of 390.3 mV, while Co NP demonstrated the highest overpotential of 459.5 mV. The overpotential for material Co@Mo₂Ti₂C₃T_x and Co@Ti₃C₂T_x were 435.7, and 451.6 mV, respectively. These findings suggest that the Co@Mo₂CT_x possesses superior OER activity compared to the other MXene support materials, while bare Co NP exhibits the lowest OER activity.

Tafel plots were analyzed to gain further insight into the OER kinetics of the electrocatalysts (Fig. 4(b)). The Tafel slope represents the rate of change of the overpotential with respect to the logarithm of the current density. The Tafel slopes for materials Co@Mo₂CT_x, Co@Mo₂Ti₂C₃T_x, Co@Ti₃C₂T_x, and bare Co NP were 57.43, 71.33, 79.22, and 88.59 mV dec⁻¹, respectively. The lower Tafel slope for Co@Mo₂CT_x indicates that it has a faster reaction kinetics for OER compared to the other hybrid samples. In contrast, bare Co NP exhibits the highest Tafel slope, indicating that it has the slowest reaction kinetics for OER among the four samples. The difference in Tafel slope suggests that each sample has different activation energies required for the OER. In general, a lower activation energy can be achieved through an increase in electrical conductivity. However, when considering that the electrical conductivities of our tested MXenes are in order of Ti₃C₂T_x > Mo₂Ti₂C₃T_x > Mo₂CT_x, which was in contrast to the order of OER kinetic activity, we surmised that a more complex interplay of atomic composition of

MXenes affects OER kinetics.

Furthermore, single cell anion exchange membrane water electrolyzers were fabricated to evaluate the practical electrocatalytic performance of the samples in a more realistic and scalable system compared to the laboratory-scale RDE test. In the AEMWE experiments (Fig. 4(c)), we evaluated the electrocatalytic activity trends of the four different types of samples, as previously discussed with the 3-electrode RDE system. PtRu/C utilization as HER catalyst of AEMWE single cell system was to prevent phenyl adsorption resulting to poisoning effect on Pt surface from ionomer (TMA-70) content with half-cell results shown in Fig. S7 [2]. The obtained polarization curves of the samples showed similar trends in terms of their current density profiles. The Co@Mo₂CT_x exhibited the highest current density at a given cell voltage (2.11 A cm^{-2} @ 1.8 V, 5.57 A cm^{-2} @ 2.0 V), indicating its superior OER activity compared to the other samples. The Co@Mo₂Ti₂C₃T_x sample showed slightly lower current density (1.49 A cm^{-2} @ 1.8 V, 4.54 A cm^{-2} @ 2.0 V) than Co@Mo₂CT_x, while the Co@Ti₃C₂T_x and bare Co NP exhibited even lower current density (0.76 and 0.88 A cm^{-2} @ 1.8 V, 2.31 and 2.27 A cm^{-2} @ 2.0 V, respectively). The polarization curve profiles of the samples provided great insight into the effect of electrical conductivity. Despite of highest electrical conductivity of Ti₃C₂T_x, Co@Ti₃C₂T_x did not show any improvement in OER activity in the AEMWE experiments. Whereas, the Co@Mo₂CT_x catalyst exhibited the highest OER activity among the samples, presumably due to the presence of unexpected Co catalyst-MXene support interactions. These interactions are speculated to synergistically increase the intrinsic OER activity of Co.

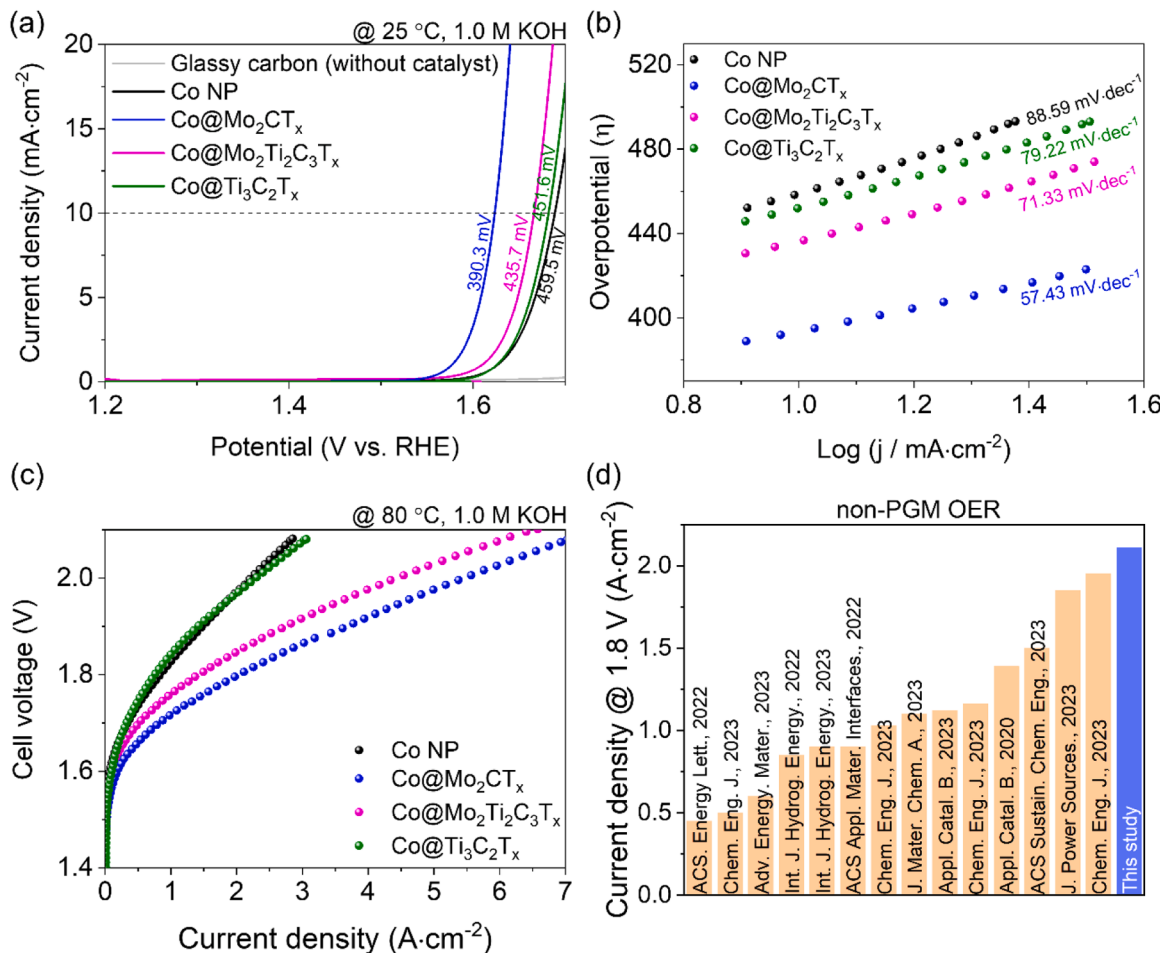


Fig. 4. Electrochemical OER data (a) LSV curves of Co NP and Co@MXene catalysts at 25 °C under 1.0 M KOH, (b) Tafel plots at three electrode system (c) polarization curves of Co NP and Co@MXene catalysts at 80 °C, supplying 1.0 M KOH and (d) recently reported AEMWE non-PGM OER data comparison at 1.8 V_{cell}. Data details are in Table. S1.

3.4. Electrochemical durability analysis and in-situ XAFS

In addition to evaluating the initial performance with polarization curve measurements, chronopotentiometry tests were also conducted on the samples to investigate their electrochemical stability over an extended period of time to evaluate their durability (Fig. 5(a)). Bare Co NP and Co@Mo₂CT_x showed excellent stability and maintained a steady voltage over the course of several hundred hours (~700), indicating their high stability as an electrocatalyst. While Co@Mo₂Ti₂C₃T_x sample also exhibited good stability, but its voltage fluctuated slightly over time and showed a device shortage at 200 h. In contrast, the Co@Ti₃C₂T_x showed poor stability, with their cell voltages increasing significantly over time with degradation rate of 200.75 μ V h⁻¹. This was mainly attributed to the variations in the types of interactions between the Co NP and various MXene supports. While the increase in cell voltage is indicative of degradation of the MXene support, the mode for which

degradation occurs can be thought to arise from either the electrochemical oxidation or corrosion in alkaline environment or the chemical oxidation of MXene under aqueous conditions [37]. The Co@Mo₂CT_x catalyst showed the highest electrochemical stability among the samples, making it a promising candidate for use in AEMWE devices.

The electrochemical impedance spectroscopy (EIS) measurements were conducted to investigate the electrochemical properties of the samples over the course of the AEMWE operation time. As shown in the Nyquist plots (Fig. S15) measured at 1.8 V, all the samples exhibited semicircles in the high-frequency region and inclined lines in the low-frequency region, indicating the presence of charge transfer resistance (R_{ct}) and mass transport resistance for OER, respectively. The R_{ct} value obtained from EIS analysis can provide information about the interfacial properties between the anode catalyst and the electrolyte, which can affect the overall performance and stability of the anode catalyst. Among the four samples, Co@Mo₂CT_x showed the lowest R_{ct} value at 0 h and

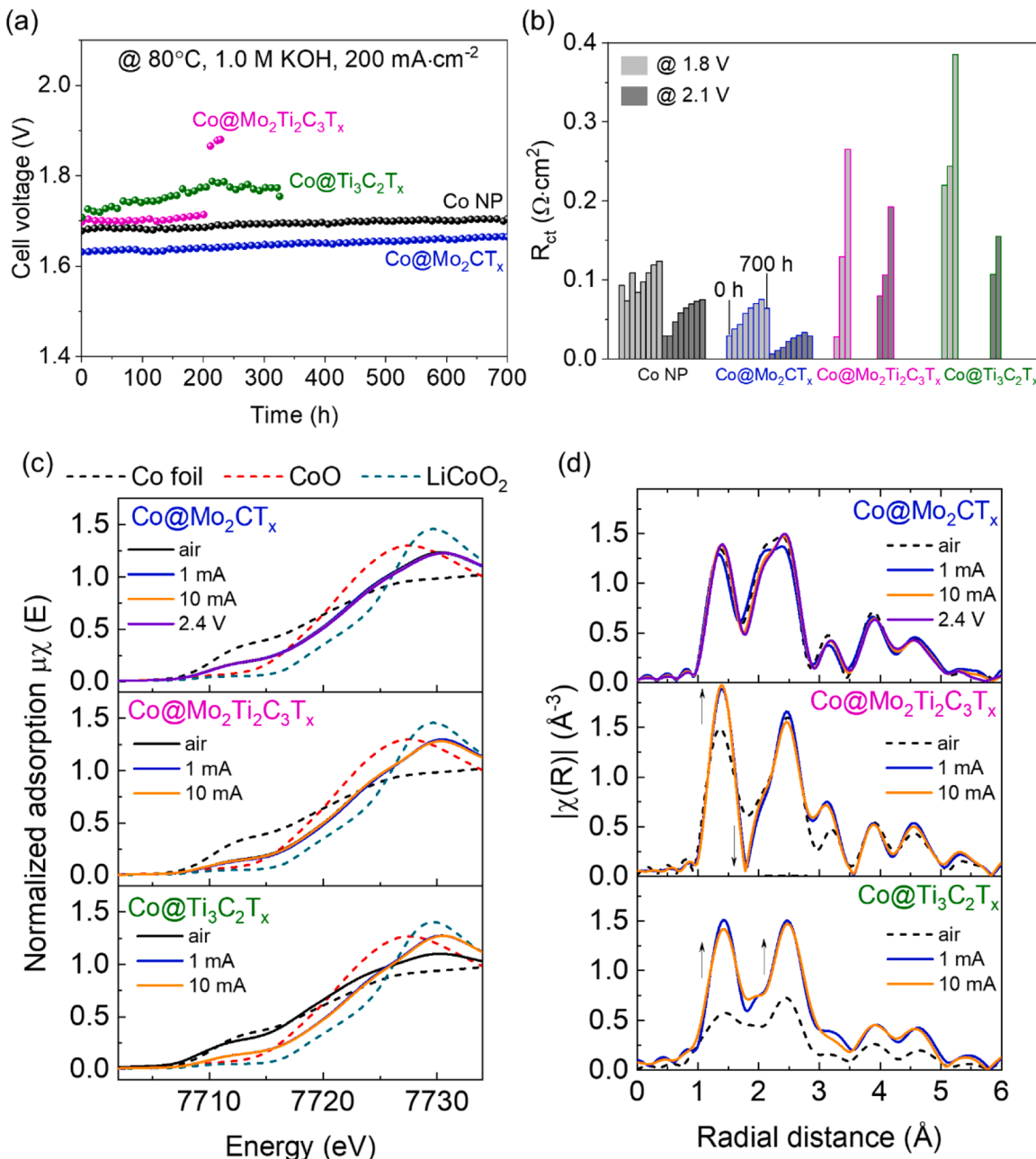


Fig. 5. (a) Electrochemical durability test at 80 °C, 1.0 M KOH, 200 mA cm⁻² for 700 h, and (b) charge transfer resistance change every 100 h at 1.8 V, and 2.1 V. In-situ Co K-edge XAS spectra of Co@MXene at non-faradaic current (1 mA cm⁻²), faradaic current (10 mA cm⁻²) in (c) XANES and (d) FT-EXAFS.

maintained the smallest R_{ct} values during the 200 h test, which implies the fast charge transfer and excellent stability of both the catalyst and its support. Meanwhile, the bare Co NP exhibited a higher R_{ct} value at 0 h and showed slight increase during the 200 h operation, indicating the sluggish reaction kinetics than Co@Mo₂CT_x due presumably to the low conductivity of the catalyst. The R_{ct} values of Co@Mo₂Ti₂C₃T_x and Co@Ti₃C₂T_x were inferior to those of Co@Mo₂CT_x and bare Co NP, reflecting the different degrees of catalyst-support interactions. In particular, while the initial R_{ct} value of Co@Mo₂Ti₂C₃T_x was similar to bare Co NP, its R_{ct} value changed drastically over the operation time and eventually reached a higher R_{ct} value.

As shown in Fig. 5(b), the change in R_{ct} value with respect to operation time and applied voltage was summarized for the four sample groups. While Co@Mo₂Ti₂C₃T_x and Co@Ti₃C₂T_x showed a significant increase in R_{ct} value over time, bare Co NP and Co@Mo₂CT_x demonstrated relatively stable R_{ct} values. Moreover, Co@Mo₂CT_x exhibited a lower R_{ct} value range and slight change compared to the other three samples. These observations suggest that the performance of the catalysts is closely related to their intrinsic properties, such as the degree of interaction between the catalyst and support materials, and not the electrical conductivity of the support materials. The observed trends with the operation time can provide useful insights into the design and optimization of highly efficient and stable electrocatalysts, which is consistent with the observed decrease in OER activity during long-term operation. Overall, the EIS results reveal that Co@Mo₂CT_x is the most efficient and stable catalyst for OER among the four samples, owing to the strong catalyst-support interactions. Moreover, we measured the hydrogen Faradaic efficiency, hydrogen production rate, and its energy conversion efficiency at 100, 200, 300, 500 mA cm⁻² using Co@Mo₂CT_x catalyst (Fig. S16). H₂ Faradaic efficiency maintained 100% except at 100 mA cm⁻², with more than 75% of energy conversion efficiency. By 700 h of AEMWE operation at 200 mA cm⁻², hydrogen could be generated 5.3 g cm⁻² or 292.6 L cm⁻² in a stable manner.

To probe the surface properties of our Co@MXene catalysts under real-time working conditions, in-situ study were carried out, as the composition and structure of the catalyst can change significantly under reaction conditions. Each catalyst was analyzed in air (without electrolyte and electrical potential), at non-faradaic current (1 mA cm⁻²), and at faradaic current (10 mA cm⁻²). Fig. 5(c) shows the XANES profiles having no oxidation state change during experiment for Co@Mo₂CT_x and Co@Mo₂Ti₂C₃T_x. Moreover, when Co@Mo₂CT_x was subjected to a further higher electrical potential to investigate the change in cobalt oxidation state, little alteration was observed. On the other hand, the Co@Ti₃C₂T_x exhibited a rapid change to a higher oxidation state immediately following applied current and it maintained this higher oxidation state, lending credence to our analysis that Ti₃C₂T_x was electrochemically oxidized over time. Co K-edge FT-EXAFS analysis also revealed a stark crystal structure change when an electrical potential was applied in real time as shown in Fig. 5(d). In contrast to Co@Ti₃C₂T_x, Co@Mo₂CT_x has minute crystal structure change of the active site Co-K edge even at the highest tested electrical potential (2.4 V vs. RHE). This meant that the active site was well-preserved under alkaline electrochemical OER environment, while Co@Mo₂Ti₂C₃T_x and Co@Ti₃C₂T_x were continuously oxidized. Evidence for this was found through the coordination number variation, indicating oxide formation on the cobalt surface for Co@Mo₂Ti₂C₃T_x, and Co@Ti₃C₂T_x. For Co@Ti₃C₂T_x, this oxide formation was noticeably severe, which can be attributed to the fact that the electrochemical oxidation is most likely initiated at the Ti-O surface, for which Co@Mo₂Ti₂C₃T_x is shielded by the surface Mo-O. These changes in cobalt structure indicate the formation of cobalt oxyhydroxide structure which already has been reported to be the most active form of cobalt in many works [38,39]. For Co@Mo₂CT_x, which already possesses mainly cobalt oxyhydroxide structure Co(OOH)@Mo₂CT_x, most likely arising from the increased defective structure Mo₂CT_x during MXene etching synthesis and Co seeding, maintained a ultra-durable Co-Mo interaction at 2.1 Å. For

Co@Mo₂Ti₂C₃T_x, and Co@Ti₃C₂T_x, a similar phenomena of the transformation into the cobalt-oxyhydroxide structure (Co(OOH) @Mo₂Ti₂C₃T_x, Co(OOH)@Ti₃C₂T_x) was also observed, but with a much larger oxidation state change reflective of irreversible MXene oxidation and eventual loss of active sites. Ongoing studies into controlling Co NP size and morphology may provide a pathway to further improving OER performance and durability in MXene-based electrocatalysts.

4. Conclusion

In conclusion, a systematic investigation into the OER performance and durability of Co@MXene catalysts with three different MXenes (Ti₃C₂T_x, Mo₂Ti₂C₃T_x, Mo₂CT_x) was carried out. A strong Mo-Co interaction between Mo₂CT_x MXene and Co NP was revealed to the main cause for the boosting of inherent OER catalytic activity of Co, characterized rigorously in both RDE and MEA tests in anion exchange membrane water electrolyzers, with Co@Mo₂CT_x reaching an impressive anion exchange water electrolysis performance of 2.11 A cm⁻² at 1.8 V with over 700 h of stable performance, exceeding previous benchmarks for non-precious group metal OER catalysts. DFT calculations and a surface properties analyzed through EXAFS and XPS supported the strong Mo-Co interaction, while bucking the traditional notion that electrical conductivity plays a major role in MXene-based electrocatalysts. We believe this study provides a new rationale for the design of MXene-based electrocatalysts through design of MXene surface interactions with active material for future energy conversion electrocatalysts.

CRediT authorship contribution statement

Hwang Seung Sang: Formal analysis. **Koh Dong-Yeon:** Project administration. **Jeon Hyo Sang:** Formal analysis. **Ahn Cheol-Hee:** Formal analysis. **Kim Seon Joon:** Formal analysis. **Choi Gwan Hyun:** Writing – review & editing, Writing – original draft, Conceptualization. **Koo Chong Min:** Writing – review & editing, Supervision, Methodology. **Ram Swetarekha:** Resources, Methodology. **In Insik:** Methodology. **Park Young Sang:** Formal analysis, Data curation, Conceptualization. **Oh Taegon:** Formal analysis. **Chae Ari:** Writing – original draft, Data curation. **Jung Jiyoong:** Formal analysis, Conceptualization. **Lee Albert S.:** Writing – review & editing, Writing – original draft, Supervision, Project administration, Conceptualization. **Lee Seung-Cheol:** Project administration, Methodology. **Bhattacharjee Satadeep:** Methodology, Funding acquisition, Conceptualization.

Declaration of Competing Interest

The authors declare that they have no known competing financial interests or personal relationships that could have appeared to influence the work reported in this paper.

Data availability

Data will be made available on request.

Acknowledgements

This work was supported by the by the National Research Council of Science & Technology (NST) grant by the Korea government (MSIT) (CRC22031-000) and the Institutional Program at KIST (2V09834). This study was also partially supported by grants from the Basic Science Research Program (2021M3H4A1A03047327 and 2022R1A2C3006227) through the National Research Foundation of Korea, funded by the Ministry of Science, ICT, and Future Planning, Republic of Korea.

Appendix A. Supporting information

Supplementary data associated with this article can be found in the online version at doi:10.1016/j.apcatb.2024.123731.

References

- [1] N. Du, C. Roy, R. Peach, M. Turnbull, S. Thiele, C. Bock, Anion-exchange membrane water electrolyzers, *Chem. Rev.* 122 (2022) 11830–11895.
- [2] D. Li, E.J. Park, W. Zhu, Q. Shi, Y. Zhou, H. Tian, Y. Lin, A. Serov, B. Zulevi, E. D. Baca, C. Fujimoto, H.T. Chung, Y.S. Kim, Highly quaternized polystyrene ionomers for high performance anion exchange membrane water electrolyzers, *Nat. Energy* 5 (2020) 378–385.
- [3] Y. Gorlin, T.F. Jaramillo, A bifunctional nonprecious metal catalyst for oxygen reduction and water oxidation, *J. Am. Chem. Soc.* 132 (2010) 13612–13614.
- [4] Y. Leng, G. Chen, A.J. Mendoza, T.B. Tighe, M.A. Hickner, C.-Y. Wang, Solid-state water electrolysis with an alkaline membrane, *J. Am. Chem. Soc.* 134 (2012) 9054–9057.
- [5] M.A. Abdulkareem, T. Wilberforce, K. Elsaid, E.T. Sayed, E.A. Abdelghani, A. Olabi, Transition metal carbides and nitrides as oxygen reduction reaction catalyst or catalyst support in proton exchange membrane fuel cells (PEMFCs), *Int. J. Hydrog. Energy* 46 (2021) 23529–23547.
- [6] G.H. Choi, M.G. Nam, S.J. Kwak, S.H. Kim, H. Chang, C.-S. Shin, W.B. Lee, P.J. Yoo, Modularly aromatic-knit graphitizable phenolic network as a tailored platform for electrochemical applications, *Energy Environ. Sci.* 14 (2021) 3203–3215.
- [7] C. Daiane Ferreira da Silva, F. Claudel, V. Martin, R. Chattot, S. Abbou, K. Kumar, I. Jiménez-Morales, S. Cavaliere, D. Jones, J. Rozière, L. Solà-Hernandez, C. Beauger, M. Faustini, J. Peron, B. Gilles, T. Encinas, L. Piccolo, F. Henrique Barros de Lima, L. Dubau, F. Maillard, Oxygen evolution reaction activity and stability benchmarks for supported and unsupported IrO_x electrocatalysts, *ACS Catal.* 11 (2021) 4107–4116.
- [8] G.H. Choi, N.C.S. Selvam, H. Kim, Y.S. Park, J. Jung, M.G. Nam, H.S. Jeon, A. S. Lee, W.-S. Yoon, P.J. Yoo, High-valent metal site incorporated heterointerface catalysts for high-performance anion-exchange membrane water electrolyzers, *Appl. Catal. B Environ.* 333 (2023) 122816.
- [9] K.K. Karuppanan, A.V. Raghu, M.K. Panthalingal, S. Ramanathan, T. Kumaresan, B. Pullithadathil, Triple phase boundary augmentation in hierarchical, Pt grafted N-doped mesoporous carbon nanofibers for high performance and durable PEM fuel cells, *J. Mater. Chem. A* 6 (2018) 12768–12781.
- [10] I.S. Filimonenkova, C. Bouillet, G. Kéranguévin, P.A. Simonov, G.A. Tsirlina, E. R. Savinova, Carbon materials as additives to the OER catalysts: RRDE study of carbon corrosion at high anodic potentials, *Electrochim. Acta* 321 (2019) 134657.
- [11] Y. Lin, K.-H. Wu, Q. Lu, Q. Gu, L. Zhang, B. Zhang, D. Su, M. Plodinec, R. Schlögl, S. Heumann, Electrocatalytic water oxidation at quinone-on-carbon: a model system study, *J. Am. Chem. Soc.* 140 (2018) 14717–14724.
- [12] C. Dai, H. Lin, G. Xu, Z. Liu, R. Wu, Y. Chen, Biocompatible 2D titanium carbide (MXenes) composite nanosheets for pH-responsive MRI-guided tumor hyperthermia, *Chem. Mat.* 29 (2017) 8637–8652.
- [13] B. Anasori, M.R. Lukatskaya, Y. Gogotsi, 2D metal carbides and nitrides (MXenes) for energy storage, *Nat. Rev. Mater.* 2 (2017) 16098.
- [14] F. Shahzad, M. Alhabeb, C.B. Hatter, B. Anasori, S. Man Hong, C.M. Koo, Y. Gogotsi, Electromagnetic interference shielding with 2D transition metal carbides (MXenes), *Science* 353 (2016) 1137–1140.
- [15] M. Naguib, V.N. Mochalin, M.W. Barsoum, Y. Gogotsi, 25th Anniversary Article: MXenes: a new family of two-dimensional materials, *Adv. Mater.* 26 (2014) 992–1005.
- [16] M. Naguib, M. Kurtoglu, V. Presser, J. Lu, J. Niu, M. Heon, L. Hultman, Y. Gogotsi, M.W. Barsoum, Two-dimensional nanocrystals produced by exfoliation of Ti₃AlC₂, *Adv. Mater.* 23 (2011) 4248–4253.
- [17] M.R. Lukatskaya, O. Mashtalir, C.E. Ren, Y. Dall'Agnesse, P. Rozier, P.L. Taberna, M. Naguib, P. Simon, M.W. Barsoum, Y. Gogotsi, Cation intercalation and high volumetric capacitance of two-dimensional titanium carbide, *Science* 341 (2013) 1502–1505.
- [18] M. Ghidu, M.R. Lukatskaya, M.-Q. Zhao, Y. Gogotsi, M.W. Barsoum, Conductive two-dimensional titanium carbide 'clay' with high volumetric capacitance, *Nature* 516 (2014) 78–81.
- [19] X. Zhao, X. Zheng, Q. Lu, Y. Li, F. Xiao, B. Tang, S. Wang, D.Y. Yu, A.L. Rogach, Electrocatalytic enhancement mechanism of cobalt single atoms anchored on different MXene substrates in oxygen and hydrogen evolution reactions, *EcoMat* 5 (2023) e12293.
- [20] D. Chanda, K. Kannan, J. Gautam, M.M. Meshesha, S.G. Jang, V.A. Dinh, B.L. Yang, Effect of the interfacial electronic coupling of nickel-iron sulfide nanosheets with layer Ti₃C₂ MXenes as efficient bifunctional electrocatalysts for anion-exchange membrane water electrolysis, *Appl. Catal. B Environ.* 321 (2023) 122039.
- [21] M. Alhabeb, K. Maleski, B. Anasori, P. Lelyukh, L. Clark, S. Sin, Y. Gogotsi, Guidelines for synthesis and processing of two-dimensional titanium carbide (Ti₃C₂T_x MXene), *Chem. Mater.* 29 (2017) 7633–7644.
- [22] K. Maleski, C.E. Shuck, A.T. Faafman, Y. Gogotsi, The broad chromatic range of two-dimensional transition metal carbides, *Adv. Opt. Mater.* 9 (2021) 2001563.
- [23] M.J. Jang, S.H. Yang, M.G. Park, J. Jeong, M.S. Cha, S.-H. Shin, K.H. Lee, Z. Bai, Z. Chen, J.Y. Lee, S.M. Choi, Efficient and durable anion exchange membrane water electrolysis for a commercially available electrolyzer stack using alkaline electrolyte, *ACS Energy Lett.* 7 (2022) 2576–2583.
- [24] H. Kim, B. Anasori, Y. Gogotsi, H.N. Alshareef, Thermoelectric properties of two-dimensional molybdenum-based MXenes, *Chem. Mater.* 29 (2017) 6472–6479.
- [25] M. Han, C.E. Shuck, R. Rakhamanov, D. Parchment, B. Anasori, C.M. Koo, G. Friedman, Y. Gogotsi, Beyond Ti₃C₂T_x: MXenes for electromagnetic interference shielding, *ACS Nano* 14 (2020) 5008–5016.
- [26] X. Dong, Y. Zhang, B. Ding, X. Hao, H. Dou, X. Zhang, Layer-by-layer self-assembled two-dimensional MXene/layered double hydroxide composites as cathode for alkaline hybrid batteries, *J. Power Sources* 390 (2018) 208–214.
- [27] J. Halim, K.M. Cook, P. Eklund, J. Rosen, M.W. Barsoum, XPS of cold pressed multilayered and freestanding delaminated 2D thin films of Mo₂Ti₂C₂T_x (MXenes), *Appl. Surf. Sci.* 494 (2019) 1138–1147.
- [28] A. Byeon, C. Hatter, J.H. Park, C.W. Ahn, Y. Gogotsi, J.W. Lee, Molybdenum oxide/carbon composites derived from the CO₂ oxidation of Mo₂CT_x (MXene) for lithium ion battery anodes, *Electrochim. Acta* 258 (2017) 979–987.
- [29] X. Lang, M.A. Qadeer, G. Shen, R. Zhang, S. Yang, J. An, L. Pan, J.-J. Zou, A Co–Mo 2 N composite on a nitrogen-doped carbon matrix with hydrogen evolution activity comparable to that of Pt/C in alkaline media, *J. Mater. Chem. A* 7 (2019) 20579–20583.
- [30] H. Lin, N. Liu, Z. Shi, Y. Guo, Y. Tang, Q. Gao, Cobalt-doping in molybdenum carbide nanowires toward efficient electrocatalytic hydrogen evolution, *Adv. Func. Mater.* 26 (2016) 5590–5598.
- [31] H. Shen, T. Peppel, J. Strunk, Z. Sun, Photocatalytic reduction of CO₂ by metal-free-based materials: recent advances and future perspective, *Sol. RRL* 4 (2020) 1900546.
- [32] J. Liu, T. Chen, P. Juan, W. Peng, Y. Li, F. Zhang, X. Fan, Hierarchical cobalt borate/MXenes hybrid with extraordinary electrocatalytic performance in oxygen evolution reaction, *ChemSusChem* 11 (2018) 3758–3765.
- [33] L.C. Seitz, D. Nordlund, A. Gallo, T.F. Jaramillo, Tuning composition and activity of cobalt titanium oxide catalysts for the oxygen evolution reaction, *Electrochim. Acta* 193 (2016) 240–245.
- [34] Y. Tsuji, K. Ogasawara, M. Kitano, K. Kishida, H. Abe, Y. Niwa, T. Yokoyama, M. Hara, H. Hosono, Control of nitrogen activation ability by Co–Mo bimetallic nanoparticle catalysts prepared via sodium naphthalene-reduction, *J. Catal.* 364 (2018) 31–39.
- [35] H. Tompkins, J. Augis, The oxidation of cobalt in air from room temperature to 467°C, *Oxid. Met.* 16 (1981) 355–369.
- [36] G.C. Anderson, B.S. Pivovar, S.M. Alia, Establishing performance baselines for the oxygen evolution reaction in alkaline electrolytes, *J. Electrochem. Soc.* 167 (2020) 044503.
- [37] X. Zhao, D.E. Holta, Z. Tan, J.-H. Oh, I.J. Echols, M. Anas, H. Cao, J.L. Lutkenhaus, M. Radovic, M.J. Green, Annealed Ti₃C₂T_x MXene films for oxidation-resistant functional coatings, *ACS Appl. Nano Mater.* 3 (2020) 10578–10585.
- [38] A. Bergmann, T.E. Jones, E. Martinez Moreno, D. Teschner, P. Chernev, M. Gliech, T. Reier, H. Dau, P. Strasser, Unified structural motifs of the catalytically active state of Co (oxyhydr) oxides during the electrochemical oxygen evolution reaction, *Nat. Catal.* 1 (2018) 711–719.
- [39] F.T. Haase, A. Bergmann, T.E. Jones, J. Timoshenko, A. Herzog, H.S. Jeon, C. Rettenmaier, B.R. Cuenya, Size effects and active state formation of cobalt oxide nanoparticles during the oxygen evolution reaction, *Nat. Energy* 7 (2022) 765–773.